IEEE Access
Multidisciplinary ⋮ Rapid Review ⋮ Open Access Journal

Received 24 May 2024, accepted 10 July 2024, date of publication 15 July 2024, date of current version 24 July 2024.

Digital Object Identifier 10.1109/ACCESS.2024.3428313

RESEARCH ARTICLE

A Novel Hybrid Acquisition System for Industrial Condition Monitoring and Predictive Maintenance

DANIEL PINARDI[1], LUCA ARPA[2], ANDREA TOSCANI[1], ELISABETTA MANCONI[1], MARCO BINELLI[1], AND EMILIANO MUCCHI[2]

[1]Department of Engineering and Architecture, University of Parma, 43124 Parma, Italy
[2]Department of Engineering, University of Ferrara, 44124 Ferrara, Italy

Corresponding author: Andrea Toscani (andrea.toscani@unipr.it)

This work was supported by the National Recovery and Resilience Plan (NRRP) Mission 4 Component 2 Investment 1.5—Call for tender No. 3277 of 30/12/2021 of Italian Ministry of University and Research through European Union—NextGenerationEU Award: Project Code ECS_00000033, Concession Decree No. 1052 of 23/06/2022, adopted by Italian Ministry of University and Research, CUP B33D21019790006, Ecosystem for Sustainable Transition of Emilia-Romagna (ECOSISTER).

ABSTRACT A novel data acquisition system for condition monitoring and predictive maintenance of mechanical parts, machinery, and industrial plants is presented. Current commercial solutions rely on an analog architecture and a star topology, in which all transducers are connected to a centralized acquisition unit. Usually this requires long shielded cables, which are sensitive to electromagnetic disturbances, always present in industrial environments. The proposed solution makes use of a digital bus implemented on an Unshielded Twisted Pair to connect one or more Acquisition Nodes to a data storage system (e.g., a laptop or an industrial computer). The wiring is simplified, cabling cost is reduced, high disturbance rejection is obtained, at the same time ensuring synchronization between all signals, mandatory for the computation of the most advanced diagnostic metrics. The performance and effectiveness of the developed system are proved in comparison with a top-quality, laboratory-grade commercial solution. A 10-days experiment was performed on a radial bearing mounted on a bearing test bench, by employing both systems side-by-side. Early-stage damage identification will be demonstrated with the described solution, despite costing a fraction and offering numerous advantages for industrial applications with respect to products currently available on the market.

INDEX TERMS Bearing fault detection, data acquisition system, digital bus, industrial condition monitoring, predictive maintenance.

I. INTRODUCTION

Many data acquisition (DAQ) systems, together with data processing algorithms, have been developed in the last decades for the detection of incipient damages before major faults occur, with the aim of improving industrial machinery maintenance. The main efforts were spent on electric machines [1] and rotating parts [2], whose failures may result in a performance reduction, efficiency loss, overheating, and increased noisiness.

Traditionally, analog DAQ systems for industrial Condition Monitoring (CM) are based on a star topology (FIGURE 1, bottom), in which each sensor is directly connected to a central acquisition unit [3], [4]. On the one hand, this ensures a perfect synchronization between all the channels, a mandatory condition for several processing techniques [5], [6]. On the other hand, the wiring becomes bulky, costly, and more subject to electromagnetic disturbances, always present in factories and industrial plants, and to which long analog cables are particularly sensitive to electromagnetic noise. High initial costs and system complexity, requiring substantial investment and extended implementation periods, are two common drawbacks of

The associate editor coordinating the review of this manuscript and approving it for publication was Nagarajan Raghavan.

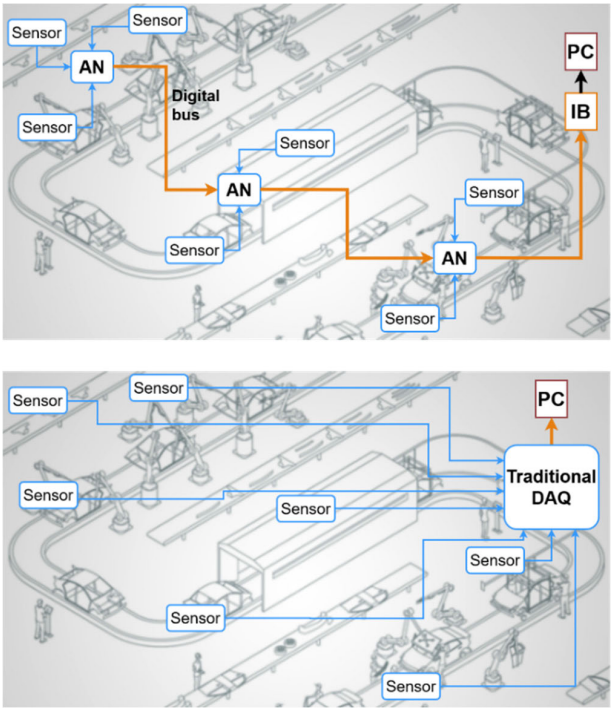

FIGURE 1. Industrial monitoring systems: the proposed daisy-chain hybrid solution (top) and a traditional star topology (bottom).

current commercial data acquisition systems for condition monitoring. Scalability is another concern, as shown in [7], especially in large-scale industrial operations, where the infrastructure required to handle vast amounts of data and numerous sensors can be expensive and difficult to maintain. Furthermore, data integration and interoperability pose additional challenges, as referred in [8]. Many commercial systems use proprietary formats and protocols, making the integration with existing infrastructure and third-party tools more complex or even not possible. Table 1 summarizes the comparison between the proposed solution and the traditional ones.

TABLE 1. Comparison of the main features of the proposed solution and traditional solutions.

Feature	Proposed solution	Traditional solution
Topology	Daisy chain, distributed system	Star, concentrated system
Signal Path	Hybrid	Full Analog
Scalability / Flexibility	High	Limited / None
Cost	Low	High
Cables	Unshielded Twisted Pair (UTP)	Shielded
Wiring complexity	Low	High

Vibration signals are commonly employed for the diagnostic of industrial plants [9] and rolling bearings [10]. The standard technique relies on the analysis of the root mean square (RMS) value, while more advanced methods make use of a statistical approach [11]. A demodulation technique, namely the envelope analysis, has proven effective in bearing fault diagnosis [12]. When a defect occurs, and the rolling elements pass over a defective area, a train of pulses appears at a characteristic frequency. The envelope allows the characteristic frequency of the bearing to be highlighted. In general, envelope analysis is a powerful tool for investigating cyclo-stationary signals (non-periodic signals with periodic statistics), such as vibratory signals from bearings. In [13], a thorough analysis of cyclo-stationary phenomena is presented accompanied by illustrative examples. The effectiveness of cyclo-stationary models in detecting faults in rotating machinery has been demonstrated in [14], where the squared envelope spectrum was employed as an indicator to evaluate 2nd order cyclo-stationary symptoms of damage. In [15], a Cyclic Wiener Filter is applied, and the filtered signal is analyzed through envelope spectrum analysis. In [16], two distinct bearing diagnostic strategies are investigated for analyzing the bearing signal. The first method makes use of the minimum entropy deconvolution and spectral kurtosis analysis [17] to enhance the impulsivity of the signal and identify the optimal spectral band for computing the signal envelope. The second method is based on a cyclo-stationary modeling approach. To enhance the identification of transients resulting from faults, [18] incorporated a probabilistic model based on Gaussian Mixtures. In [19], a technique was presented for selecting the demodulation frequency band that is optimal by utilizing the kurtosis of envelope spectrum amplitudes to detect impulses that decrease the signal-to-noise ratio. In [20], the authors examined the relationship between kurtosis-based indexes and envelope analysis in diagnosing incipient faults in rolling bearing elements. The study demonstrated analytical equivalences between the squared envelope spectrum and kurtosis of corresponding band-pass filtered analytic signals, emphasizing the inherent connection between these methodologies.

The significance of data collection in the context of Condition Based Maintenance has made it necessary to develop and implement reliable acquisition systems that enable the recording and processing of information from sensors in real-time. Additionally, the utilization of robust data analysis algorithms has facilitated the development of data-driven models for CM and predicting Remaining Useful Life (RUL). Reference [21] outlines four essential processes for a machinery prognostic program: data acquisition, health indicator (HI) construction, health stage (HS) division, and RUL prediction. Accelerated tests are a valuable tool for collecting data that represents the entire life of the observed system and can be used for further research. Bearings are a critical component for machine operation and numerous accelerated test data sets have been collected over the last two decades to provide information on their degradation processes [20], [21], [22]. Furthermore, a significant amount of data is required for the implementation of Artificial Intelligence solutions for the diagnosis and prognosis of rolling-element bearings through the utilization of pattern recognition and machine learning or deep learning algorithms [25].

In our study, an accelerated test was carried out to demonstrate the effectiveness and reliability of the presented acquisition system in carrying out a long-term test campaign. The discrete time analytical signal was obtained by applying a Hilbert transform [26] on the signal, previously bandpass filtered. Since at low frequencies the characteristic frequencies can be hidden by other vibratory phenomena, this analysis is typically conducted at high frequencies, applying a bandpass frequency filter around a resonance zone. The test rig employed in this study was previously employed by the same authors to validate a physics-based prognostics algorithm presented in [27] and a procedure for tuning a lumped parameter bearing model [28].

In this paper, an innovative DAQ system is proposed for industrial condition monitoring and predictive maintenance applications. It features a hybrid architecture, consisting of an analog Acquisition Node (AN) integrating the Analog-to-Digital (A/D) conversion and a transceiver to route the signals to a digital bus. Such a solution allows for the acquisition of high-quality piezoelectric sensors [29], [30], at the same time reducing at most the length of the analog cables, which in turn are only required to connect the sensors to the AN (FIGURE 1, top). The signals are then delivered to the storage system (typically a personal or an industrial computer) over the digital bus, which is inherently more robust to electromagnetic disturbance than any analog transmission.

The proposed system is first compared with a top-quality, laboratory grade solution, demonstrating the same performance in terms of self-noise and sensitivity. Then, the results of an experimental campaign aimed at condition monitoring via accelerometer signals of a self-aligning ball bearing installed on a test bench will be presented. The post-processing techniques include a standard approach based on RMS values and an envelope analysis. Also, in this case, it will be shown that the proposed hybrid solution provided the same results as a widely diffused commercial product.

The paper is arranged as follows: Section II describes the new hybrid DAQ system, Section III presents a validation between the proposed solution and a laboratory grade product, and Section IV presents the results of the experimental campaign on the bearing test bench. Eventually, the conclusions are reported in Section V.

II. SYSTEM OVERVIEW

The presented hybrid DAQ system makes use of the Automotive Audio Bus (A^2B), a digital communication protocol developed by Analog Devices [31]. It carries up to 32 acquisition channels at a sampling frequency (f_s) of 48 kHz on an Unshielded Twisted Pair (UTP). The connection is a daisy-chain, a feature that allows overcoming the star topology and the common limitations associated with analog wiring (bulkiness, expense, electrical noise sensitivity). The A^2B bus synchronizes all the channels with a negligible jitter [32] and a deterministic latency of about 50 μs. The propagation latency can also be compensated by the temporal alignment of the clock signals with a resolution of about 20 ns. For these reasons, the A^2B bus can provide several advantages in many other fields rather than the automotive industry, such as, but not limited to, microphone arrays [33], [34], loudspeaker arrays [35], and Structural Health Monitoring (SHM) [31], [32], [33].

The proposed Acquisition Node features a single chip AD1278 by Analog Devices to perform the A/D conversion. Up to 8 sensors can be acquired together, such as Integrated Electronic Piezoelectric (IEPE), Integrated Circuit-Piezoelectric (ICP), or any other voltage output sensors. Table 2 summarizes the main characteristics of the A/D converter.

TABLE 2. A/D Converter AD1278.

Specification	Value
Architecture	24-bit delta-sigma
Number of channels	8-ch, simultaneous sampling
Sampling rate	up to 144 kS/s
Bandwidth	70 kHz
Signal to noise ratio (SNR)	111 dB
DC accuracy – offset drift	0.8 uV/ºC
DC accuracy – gain drift	1.3 ppm/ºC
Serial interface	SPI or frame sync

After the A/D conversion, the signals are routed to the bus by an A^2B transceiver through an Integrated Interchip Sound (I^2S) interface. The AN board has been designed to accommodate several settings, individually controllable for each channel:

- Electrical Coupling. DC coupling for analog Micro Electro-mechanical Systems (MEMS) sensors, e.g. for SkyMEMS MAS1000H, or AC coupling, e.g. for piezoelectric accelerometers and microphones.
- IEPE power supply ON/OFF.
- Input voltage range ($\pm$10 V, $\pm$5 V, $\pm$2.5 V, $\pm$1.25 V, $\pm$0.625 V, $\pm$0.3125 V).

The power supply (up to 2.7 W) that is required by the AN and by the ICP/IEPE sensors is delivered by the A^2B bus itself on the same UTP cable.

III. SYSTEM VALIDATION

The Acquisition Node was experimentally compared with a top-grade solution for validation. The chosen reference system is well-established and widely recognized in the scientific community for its accuracy, proven performance, and reliability in providing high-quality data. Three kinds of tests will be presented: background noise, calibration, and measurement on a tapered bearing test bench. The authors made all the acquired data available in [38].

A. EXPERIMENTAL SETUP

Validation experiments have been performed in comparison with a Siemens SCADAS type SC-305. The analog

input stage of the two systems has been configured in AC coupling, with the same ±5 V voltage range. The employed sensor was a piezoelectric accelerometer, PCB Piezotronics type 353B18, whose specifications are reported in Table 3.

TABLE 3. Piezoelectric sensor PCB 353B18.

Specification	Value
Sensitivity	10.4 mV/g
Measurement range	±500 g peak
Frequency range	1 Hz – 10 kHz
Maximum Output Voltage	±5 V
Noise Power Spectral Density (10 Hz)	6867 $(\mu m/s^2)/\sqrt{Hz}$
Noise Power Spectral Density (100 Hz)	1766 $(\mu m/s^2)/\sqrt{Hz}$
Noise Power Spectral Density (1000 Hz)	628 $(\mu m/s^2)/\sqrt{Hz}$

To deliver the ICP power supply to the sensor without injecting it into the input stages, the ICP was disabled on both DAQ systems, and an external power supply was employed, a PCB 483A, which outputs the signal without power. The output signal was then split with a T-connector of type Bayonet Neill Concelman (BNC).

The first test consisted of acquiring 30 s of background noise. Then, the accelerometer was mounted on an accelerometer calibrator, a Bruel&Kjaer type 4294, which embodies an electromagnetic exciter driven by a crystal oscillator at a frequency of 159.15 Hz (1000 rad/s) at a standard acceleration level of 10 m/s^2. Also, in this second setup, a 30 s length signal was measured with both systems. Finally, the accelerometer was placed over the external cage of a brand-new tapered bearing mounted on the bearing test bench. Two tests, each one having a duration of 30 s, were performed at two different rotor mechanical speeds, 900 rpm and 1500 rpm. The associated frequencies can be easily derived as $F_r = rpm/60$, hence obtaining $F_r = 15$ Hz and $F_r = 25$ Hz for the two cases.

The Siemens SCADAS system was set at sampling frequency $f_s = 51.2$ kHz, while the AN at $f_s = 48$ kHz, which is the current standard sampling frequency for audio systems. Then, SCADAS recordings were down sampled to 48 kHz in post processing.

B. DISCUSSION OF THE RESULTS

Results are shown in terms of spectral analysis, covering the frequency range 5 Hz – 5 kHz. The spectra are calculated over the entire length of measured signals by means of the Fast Fourier Transform (FFT) averaged over multiple blocks, each of them having a length of 48000 samples, with Hann windowing, and 75% overlap. Hence, the frequency resolution is 1 Hz. The vertical axis of the spectra is converted in dB referred to the reference value of the International System (I.S.) for acceleration, that is 10^{-6} m/s^2.

At first, the background noise recordings were compared, and the results are shown in FIGURE 2. One can note the results are almost identical for the two systems. The Siemens

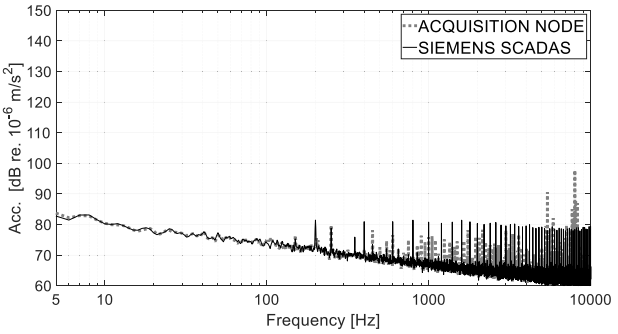

FIGURE 2. Frequency analysis of background noise.

SCADAS shows a disturbance at 200 Hz and its multiples, while the AN has a similar behavior at 150 Hz and its multiples.

Then, the calibrator signal was analyzed, and the results are shown in FIGURE 3. Also, in this case, the two systems acquired the same signals. The three main components, which are the fundamental frequency $F_c = 159.15$ Hz, and the first and second harmonics distortions, $2F_c = 318.3$ Hz, and $3F_c = 477.45$ Hz, are perfectly superimposed.

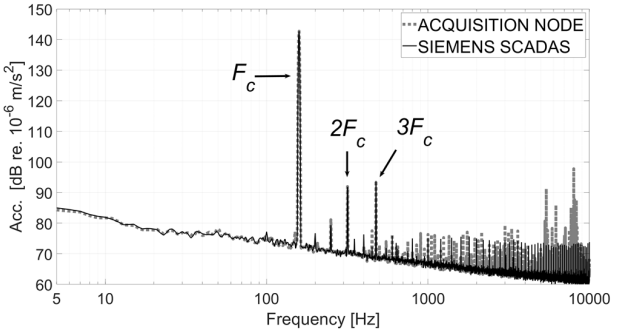

FIGURE 3. Frequency analysis of the calibration signal at $F_c = 159.15$ Hz.

Eventually, the two measurements on the brand-new tapered bearing were processed, as shown in FIGURE 4 and FIGURE 5. Even in these cases, the spectra are identical. The rotor mechanical frequencies F_r and its multiples, $2F_r$, $3F_r$ etc. are clearly distinguishable.

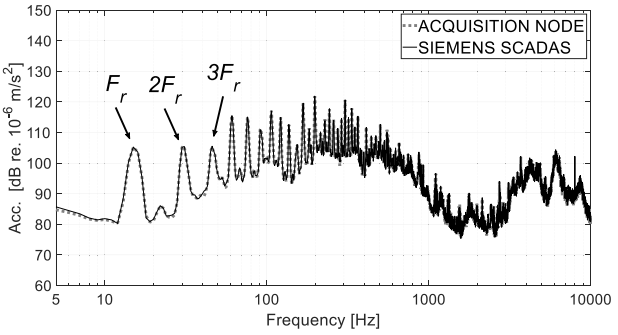

FIGURE 4. Frequency analysis of a brand-new radial bearing at $F_r = 15$ Hz.

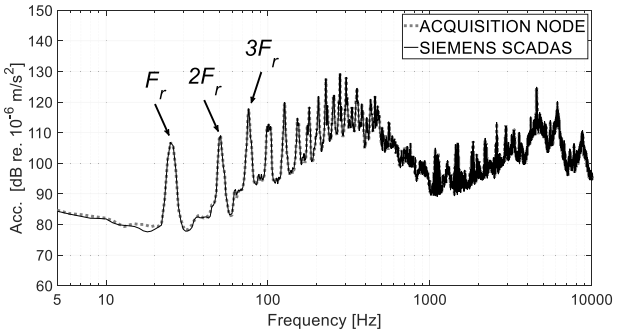

FIGURE 5. Frequency analysis of a brand-new radial bearing at $F_r = 25$ Hz.

IV. BEARING TEST BENCH

In this section, the performance of the AN is compared with a commercial product, for the predictive diagnosis of a rolling bearing installed on a bearing test bench. The authors made all the acquired data available in [39].

A. EXPERIMENTAL SETUP

The predictive fault diagnosis experiment on a self-aligning, double-row ball bearing, model 1205 ETN9, was performed in comparison with a widely employed commercial product, a National Instrument (NI) compactRIO (cRIO) controller, equipped with a 9234-module provided with four analog channels. The measurement was performed on a bearing test bench (FIGURE 6), whose specifications are reported in Table 4. The test bench features a leverage system to provide a preload to the bearing under test, with the aim of shortening the duration of the test, and a compression load cell to measure the extent of the preload with precision. For the present work, a preload of 4000 N was employed.

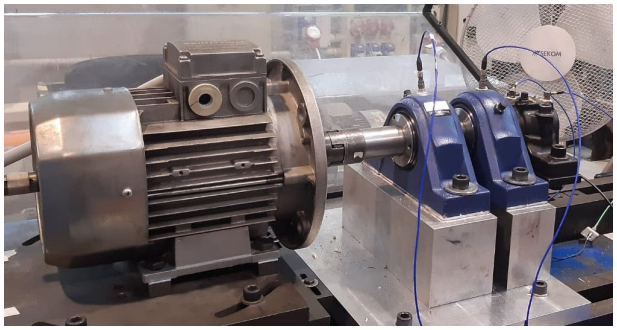

FIGURE 6. Side view of the bearing test bench.

The AN was set at sampling frequency $f_s = 48$ kHz, while the NI cRIO system at $f_s = 51.2$ kHz, and then down sampled to 48 kHz in post processing. Each system acquired a chunk of signal of five seconds length every five minutes, for the entire duration of the test, which ended after 112 h, at the complete failure of the bearing.

Coming to the radial bearing condition monitoring, different frequencies arise depending on the localization of the damage on the different parts of the bearing, such as the rolling elements, the inner ring, or the outer ring (FIGURE 7).

TABLE 4. Bearing test bench.

Specification	Value
Nominal Power	9.2 kW
Number of Poles	4
Nominal Current	19.3 A
Nominal Torque	61 Nm
Mechanical Speed	2400 rpm
Bearing preload	4000 N

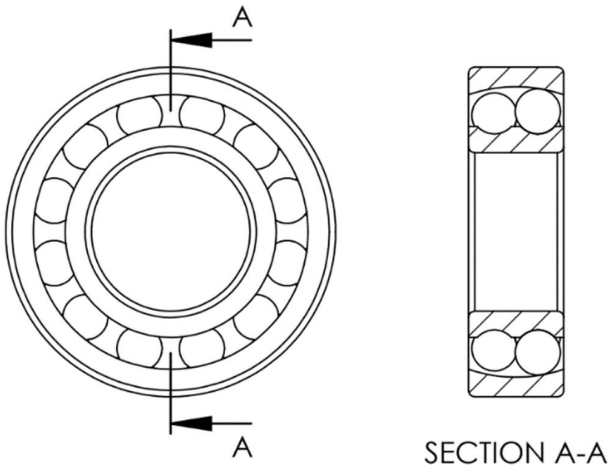

FIGURE 7. Tested bearing, model 1205 ETN 9.

These frequencies also vary with the geometry and the relative speed between the outer and the inner rings. The main four fault signatures are known as Ball Pass Frequency Outer (BPFO), Ball Pass Frequency Inner (BPFI), Ball Spin Frequency (BSF), and Fundamental Train Frequency (FTF). The analytical formulas of the above defects are well known from the theory, e.g. in [40]. They are usually derived by considering the outer ring fixed to the frame. Under this hypothesis, it follows:

$$BPFO = F_r \frac{N_B}{2}\left(1 - \frac{B_d}{P_d}\cos\beta\right) \quad (1)$$

$$BPFI = F_r \frac{N_B}{2}\left(1 + \frac{B_d}{P_d}\cos\beta\right) \quad (2)$$

$$BSF = F_r \frac{P_d}{B_d}\left(1 - \left(\frac{B_d}{P_d}\cos\beta\right)^2\right) \quad (3)$$

$$FTF = F_r \frac{1}{2}\left(1 - \frac{B_d}{P_d}\cos\beta\right) \quad (4)$$

where F_r is the rotor mechanical frequency, N_B is the number of rolling elements, B_d is the rolling element diameter, β is the contact angle, and P_d is the pitch diameter. The latter is calculated as the average between the outer and the inner

rings diameters:

$$P_d = \frac{D_o + D_i}{2} \tag{5}$$

where D_o and D_i are the diameters of the outer and inner rings, respectively. In the present work, being the rotor speed equal to 2400 rpm, it was $F_r = 40$ Hz. The specifications of the tapered bearing employed for the test can be seen in Table 5. By introducing the values reported in Table 5 in (1), (2), (3), (4), and (5), for $F_r = 40$ Hz and under the hypothesis of perfect contact angle, that is $\beta = 0°$, the expected fault frequencies were calculated for the bearing employed in the test, and they are summarized in Table 6.

TABLE 5. Tapered bearing of the experiment.

Specification	Value
D_i, inner ring diameter	25 mm
D_o, outer ring diameter	52 mm
P_d, pitch diameter	38.95 mm
N_B, number of rolling elements	12 each row
B_d, rolling element diameter	7.12 mm

TABLE 6. Calculate fault frequencies for the bearing under test at $F_r = 40$ Hz.

Specification	Value
BPFO	197 Hz
BPFI	284 Hz
BSF	103 Hz
FTF	16 Hz

It was opted to acquire two different mono-axial accelerometers, with the same specifications as in Table 3, to also evaluate the effect of different positioning. The sensors were installed on the opposite sides of the rotation axis, and each one was acquired by one of the two systems used in the test. In particular, the one marked as "A" in FIGURE 8 was connected to the AN, and the one marked as "B" in FIGURE 8 was connected to the NI DAQ.

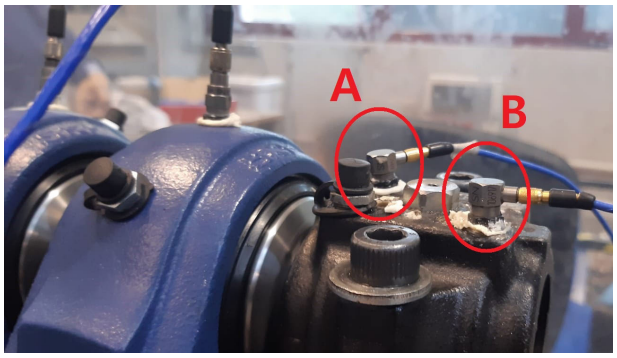

FIGURE 8. Detail view of the sensors mounting. Sensor A is connected to the AN system, sensor B is connected to the NI system.

B. DISCUSSION OF THE RESULTS

First, the RMS values of the recorded signals were compared (FIGURE 9) to assess that both systems worked correctly during the entire duration of the experiment. One can note a good superimposition of the two curves, proving that both systems recorded the same time history. A difference can be observed only at the end of the experiment, and this effect can be addressed by the positioning of the sensors. A significant increase of the RMS value at time $t = 108$ h clearly indicates the bearing failure. However, such a basic analysis method only provides an indication of the damage at an advanced or full-blown stage, when the faulty condition can be detected also by a personal inspection, due to the strong rattling noise produced by the broken part. As expected, the RMS value demonstrated not to be suitable for detecting damage at the incipient stage.

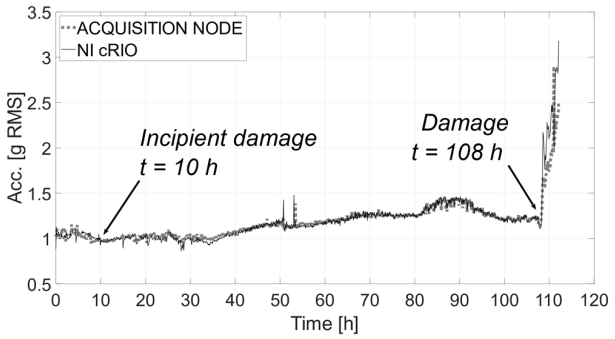

FIGURE 9. Comparison of the RMS values of the signals recorded with AN and NI during the entire time history of the experiment.

Then, the spectra of a chunk of signal having five seconds length recorded at $t = 10$ h (apparent healthy condition, FIGURE 10) and at $t = 108$ h (full-blown faulty condition, FIGURE 11) were compared. The spectra are calculated over the entire length of the chunk of signal by means of multiple FFTs averaging over blocks of 48000 samples each one, with Hann windowing, and 75% overlap. Hence, the frequency resolution is 1 Hz.

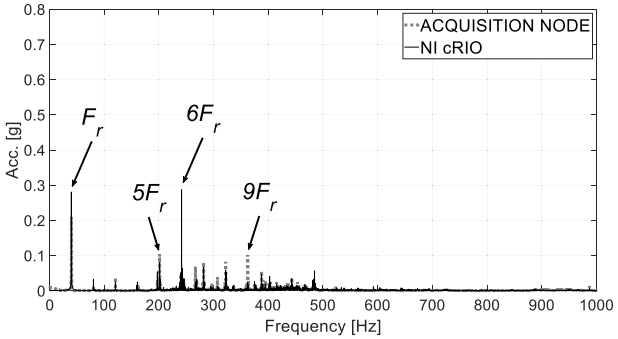

FIGURE 10. Comparison of the healthy condition spectra recorded with AN and NI at t = 10 h.

Also in this case, only the fundamental mechanical frequency F_r and its multiples can be seen at $t = 10$ h,

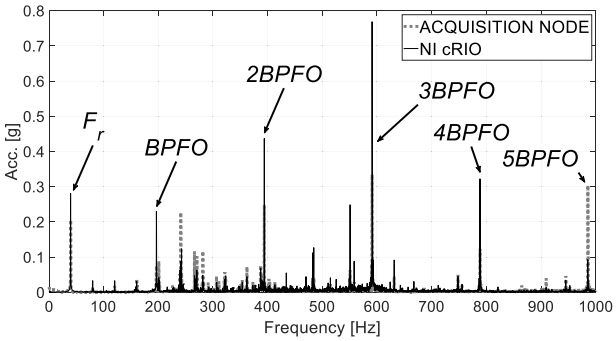

FIGURE 11. Comparison of the faulty condition spectra recorded with AN and NI at t = 108 h.

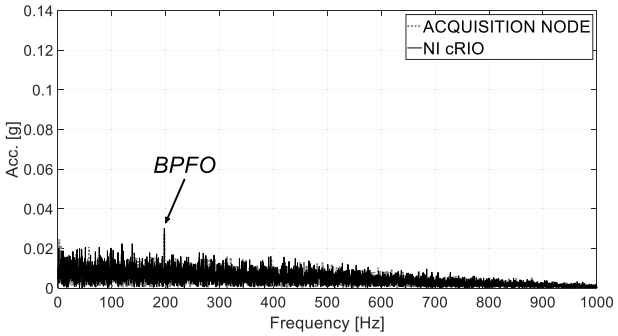

FIGURE 12. Comparison of the envelope spectra recorded with AN and NI at t = 10 h.

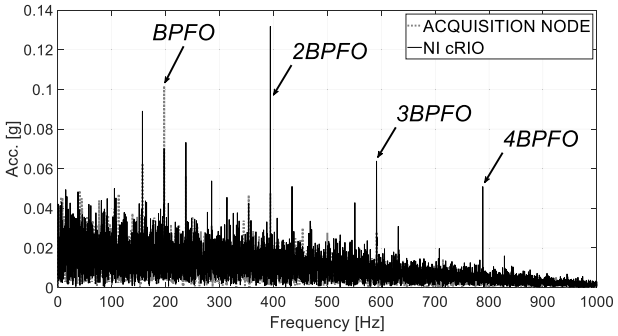

FIGURE 13. Comparison of the envelope spectra recorded with AN and NI at t = 108 h.

and no further indication of a damage at an early stage can be observed on the (apparent) healthy condition. At $t = 108\ h$, instead, it can be noted the appearance of a frequency component at 197 Hz, which corresponds to the fundamental frequency of the BPFO fault, previously calculated and reported in Table 6. The higher harmonics can also be seen at integer multiples of the BPFO fundamental frequency, at 384 Hz, 591 Hz, 788 Hz, and 985 Hz. Hence, it can be assumed that a defect has originated in the outer ring. However, at $t = 108\ h$ the damage was already at an advanced stage, clearly detectable by human inspection or with a basic processing technique such as the RMS value, as previously shown.

In both cases, a larger amplitude of the interested frequency components is observed for the spectrum of the NI system. This can be explained with the better positioning of the sensor compared to the one acquired with the AN system.

Eventually, the envelope analysis, using Hilbert transform technique, was performed on the healthy condition recording at $t = 10\ h$ to detect the failure at an incipient stage. Several benefits arise from performing amplitude demodulation using Hilbert transform techniques, whereby the one-sided spectrum is inversely transformed to the time domain [12]. This results in the generation of a complex time signal, i.e. the analytic signal, whose imaginary part is the Hilbert transform of the real part [41]. An immediate advantage is that the extraction of the spectrum's section to be demodulated is effectively achieved by an ideal filter, thus allowing for the separation of the extracted spectrum from adjacent components that might be stronger.

For this purpose, the signal was initially bandpass filtered in a resonance zone, at 8 kHz. Then, the analytic signal, i.e. the envelope, was obtained by applying the Hilbert transform to the filtered signal. The comparison between AN and NI systems is shown in Fig. 12. One can clearly note the BPFO fault frequency at 197 Hz, which has been correctly detected with both systems at an incipient stage, while neither the RMS value nor the FFT analysis provided any damage indication at $t = 10\ h$.

For the sake of completeness, the same envelope analysis was repeated also on the fault condition at $t = 108\ h$. The comparison between AN and NI systems for this case is shown in Fig. 13. One can note the BPFO fault frequency at 197 Hz (the amplitude is significantly larger with respect to the healthy condition at $t = 10\ h$) and its multiples at 384 Hz, 591 Hz, and 788 Hz.

V. CONCLUSION

A hybrid DAQ system for industrial CM and predictive maintenance of machinery and mechanical parts was presented. The described solution is based on the A^2B digital bus, which allows for connecting a series of Acquisition Node in an open loop daisy chain. Each AN is provided with analog inputs for A/D conversion and the A^2B transceiver to transmit the signals to the storage system through the digital bus.

This solution allows for acquiring high-quality, laboratory grade piezoelectric sensors, at the same time offering a series of advantages with respect to traditional systems, such as but not limited to data synchronization, fast and easy installation, high electromagnetic disturbance rejection, and reduction of the length, cost, and complexity of the cabling. In fact, traditional analog DAQ systems are usually based on star topology, which entails long analog cables, making the wiring bulky, costly, and sensitive to electromagnetic disturbances, as well as more complex and time-consuming installations.

The proposed hybrid DAQ system was validated in comparison with a widely recognized top-quality laboratory solution, a SCADAS system by Siemens. An electrical test and an experimental measurement with an accelerometer

calibrator were presented, showing the same performance in terms of self-noise and sensitivity between the two systems.

Eventually, the solution presented in this work was employed for an experiment of predictive diagnostic performed on a radial bearing installed on a test bench. In this case, the system was compared against a widely diffused commercial solution by National Instruments. The two systems recorded almost the same time history, and minimum differences were due to the different positioning of the sensors. The analysis of the acquired vibration signals was first performed with the standard RMS and FFT methods, and then with the envelope algorithm. Only the latter allowed us to identify a Ball Pass Frequency Outer fault at an incipient stage (after 10 hours of operation), while the RMS and FFT analysis detected the damage only at a full-blown stage, close to the end of the experimental campaign (after 108 hours). This result was obtained with both the commercial system and the new hybrid DAQ system presented in the manuscript, which proved to be an effective, convenient, and practical solution for condition monitoring and predictive maintenance in industry applications.

REFERENCES

[1] A. Garcia-Perez, R. d. J. Romero-Troncoso, E. Cabal-Yepez, and R. A. Osornio-Rios, "The application of high-resolution spectral analysis for identifying multiple combined faults in induction motors," *IEEE Trans. Ind. Electron.*, vol. 58, no. 5, pp. 2002–2010, May 2011, doi: 10.1109/TIE.2010.2051398.

[2] A. H. Bonnett, "Root cause AC motor failure analysis with a focus on shaft failures," *IEEE Trans. Ind. Appl.*, vol. 36, no. 5, pp. 1435–1448, Oct. 2000, doi: 10.1109/28.871294.

[3] G. Weiming, Z. Ming, G. Xinfeng, D. Yongsheng, D. Jinqi, and Z. Yizhong, "Vibration data acquisition and fault diagnosis system of hydro turbine based on CompactRIO," in *Proc. 5th Int. Conf. Mech., Automot. Mater. Eng. (CMAME)*, Aug. 2017, pp. 319–323, doi: 10.1109/CMAME.2017.8540176.

[4] M. E. Haque, M. F. M. Zain, M. A. Hannan, M. Jamil, and M. H. Johari, "Transmission loss computed of star topology sensor network base on DT, RED and SFQ buffer mechanism for overseeing high rise building structural health," *Int. J. Biosci., Biochem. Bioinf.*, vol. 3, pp. 646–649, Jan. 2013, doi: 10.7763/ijbbb.2013.v3.294.

[5] A. Abdaoui, T. M. El Fouly, and M. H. Ahmed, "Impact of time synchronization error on the mode-shape identification and damage detection/localization in WSNs for structural health monitoring," *J. Netw. Comput. Appl.*, vol. 83, pp. 181–189, Apr. 2017, doi: 10.1016/j.jnca.2017.01.004.

[6] S. Gao, X. Zhang, C. Du, and Q. Ji, "A multichannel low-power wide-area network with high-accuracy synchronization ability for machine vibration monitoring," *IEEE Internet Things J.*, vol. 6, no. 3, pp. 5040–5047, Jun. 2019, doi: 10.1109/JIOT.2019.2895158.

[7] A. Toscani, F. Immovilli, D. Pinardi, and L. Cattani, "A novel scalable digital data acquisition system for industrial condition monitoring," *IEEE Trans. Ind. Electron.*, vol. 71, no. 7, pp. 7975–7985, Jul. 2024, doi: 10.1109/TIE.2023.3301521.

[8] R. Nasfi, A. Bronselaer, and G. De Tré, "A novel approach to assess and improve syntactic interoperability in data integration," *Inf. Process. Manage.*, vol. 60, no. 6, Nov. 2023, Art. no. 103522, doi: 10.1016/j.ipm.2023.103522.

[9] D. C. Mazur, J. A. Kay, and K. D. Mazur, "Advancements in vibration monitoring for the mining industry," in *Proc. IEEE Ind. Appl. Soc. Annu. Meeting*, Oct. 2014, pp. 1–8, doi: 10.1109/IAS.2014.6978459.

[10] J. R. Stack, T. G. Habetler, and R. G. Harley, "Fault signature modeling and detection of inner race bearing faults," in *Proc. IEEE Int. Conf. Electric Mach. Drives*, May 2005, pp. 271–277, doi: 10.1109/IEMDC.2005.195734.

[11] J. Yu, "Local and nonlocal preserving projection for bearing defect classification and performance assessment," *IEEE Trans. Ind. Electron.*, vol. 59, no. 5, pp. 2363–2376, May 2012, doi: 10.1109/TIE.2011.2167893.

[12] R. B. Randall and J. Antoni, "Rolling element bearing diagnostics—A tutorial," *Mech. Syst. Signal Process.*, vol. 25, no. 2, pp. 485–520, Feb. 2011, doi: 10.1016/j.ymssp.2010.07.017.

[13] J. Antoni, "Cyclostationarity by examples," *Mech. Syst. Signal Process.*, vol. 23, no. 4, pp. 987–1036, May 2009, doi: 10.1016/j.ymssp.2008.10.010.

[14] P. Borghesani, P. Pennacchi, R. Ricci, and S. Chatterton, "Testing second order cyclostationarity in the squared envelope spectrum of non-white vibration signals," *Mech. Syst. Signal Process.*, vol. 40, no. 1, pp. 38–55, Oct. 2013, doi: 10.1016/j.ymssp.2013.05.012.

[15] Y. Ming, J. Chen, and G. Dong, "Weak fault feature extraction of rolling bearing based on cyclic Wiener filter and envelope spectrum," *Mech. Syst. Signal Process.*, vol. 25, no. 5, pp. 1773–1785, Jul. 2011, doi: 10.1016/j.ymssp.2010.12.002.

[16] D. Abboud, M. Elbadaoui, W. A. Smith, and R. B. Randall, "Advanced bearing diagnostics: A comparative study of two powerful approaches," *Mech. Syst. Signal Process.*, vol. 114, pp. 604–627, Jan. 2019, doi: 10.1016/j.ymssp.2018.05.011.

[17] R. B. Randall, *Vibration-based Condition Monitoring*. Hoboken, NJ, USA: Wiley, 2011, doi: 10.1002/9780470977668.

[18] G. Xin, N. Hamzaoui, and J. Antoni, "Semi-automated diagnosis of bearing faults based on a hidden Markov model of the vibration signals," *Measurement*, vol. 127, pp. 141–166, Oct. 2018, doi: 10.1016/j.measurement.2018.05.040.

[19] T. Barszcz and A. Jabłoński, "A novel method for the optimal band selection for vibration signal demodulation and comparison with the kurtogram," *Mech. Syst. Signal Process.*, vol. 25, no. 1, pp. 431–451, Jan. 2011, doi: 10.1016/j.ymssp.2010.05.018.

[20] P. Borghesani, P. Pennacchi, and S. Chatterton, "The relationship between kurtosis- and envelope-based indexes for the diagnostic of rolling element bearings," *Mech. Syst. Signal Process.*, vol. 43, nos. 1–2, pp. 25–43, Feb. 2014, doi: 10.1016/j.ymssp.2013.10.007.

[21] Y. Lei, N. Li, L. Guo, N. Li, T. Yan, and J. Lin, "Machinery health prognostics: A systematic review from data acquisition to RUL prediction," *Mech. Syst. Signal Process.*, vol. 104, pp. 799–834, May 2018, doi: 10.1016/j.ymssp.2017.11.016.

[22] J. Lee, H. Qiu, G. Yu, and J. Lin. *Bearing Data Set, NASA Prognostics Data Repository*. Accessed: Mar. 22, 2024. [Online]. Available: https://data.nasa.gov/download/brfb-gzcv/application%2Fzip

[23] P. Nectoux, R. Gouriveau, K. Medjaher, E. Ramasso, B. Chebel-Morello, N. Zerhouni, and C. Varnier, "PRONOSTIA: An experimental platform for bearings accelerated degradation tests," in *Proc. IEEE Int. Conf. Prognostics Health Manage.*, Jun. 2012, pp. 1–8.

[24] B. Wang, Y. Lei, N. Li, and N. Li, "A hybrid prognostics approach for estimating remaining useful life of rolling element bearings," *IEEE Trans. Rel.*, vol. 69, no. 1, pp. 401–412, Mar. 2020, doi: 10.1109/TR.2018.2882682.

[25] Y. Zhao, M. Zhou, X. Xu, and N. Zhang, "Fault diagnosis of rolling bearings with noise signal based on modified kernel principal component analysis and DC-ResNet," *CAAI Trans. Intell. Technol.*, vol. 8, no. 3, pp. 1014–1028, Sep. 2023, doi: 10.1049/cit2.12173.

[26] L. Marple, "Computing the discrete-time 'analytic' signal via FFT," *IEEE Trans. Signal Process.*, vol. 47, no. 9, pp. 2600–2603, Sep. 1999, doi: 10.1109/78.782222.

[27] A. Gabrielli, M. Battarra, E. Mucchi, and G. Dalpiaz, "Physics-based prognostics of rolling-element bearings: The equivalent damaged volume algorithm," *Mech. Syst. Signal Process.*, vol. 215, Jun. 2024, Art. no. 111435, doi: 10.1016/j.ymssp.2024.111435.

[28] A. Gabrielli, M. Battarra, E. Mucchi, and G. Dalpiaz, "A procedure for the assessment of unknown parameters in modeling defective bearings through multi-objective optimization," *Mech. Syst. Signal Process.*, vol. 185, Feb. 2023, Art. no. 109783, doi: 10.1016/j.ymssp.2022.109783.

[29] P. Jiao, K.-J.-I. Egbe, Y. Xie, A. Matin Nazar, and A. H. Alavi, "Piezoelectric sensing techniques in structural health monitoring: A state-of-the-art review," *Sensors*, vol. 20, no. 13, p. 3730, Jul. 2020, doi: 10.3390/s20133730.

[30] M. B. Moffett and J. M. Powers, "Noise in piezoelectric sensors," *J. Acoust. Soc. Amer.*, vol. 88, no. S1, p. S160, Nov. 1990, doi: 10.1121/1.2028709.

[31] Analog Devices. *A2B Audio Bus: An Easier, Simpler Solution for Audio Design*. Accessed: May 2024. [Online]. Available: https://www.analog.com/en/applications/technology/a2b-audio-bus.html
[32] N. Rocchi, A. Toscani, G. Chiorboli, D. Pinardi, M. Binelli, and A. Farina, "Transducer arrays over A^2B networks in industrial and automotive applications: Clock propagation measurements," *IEEE Access*, vol. 9, pp. 118232–118241, 2021, doi: 10.1109/ACCESS.2021.3106710.
[33] D. Pinardi, A. Toscani, M. Binelli, L. Saccenti, A. Farina, and L. Cattani, "Full-digital microphone meta-arrays for consumer electronics," *IEEE Trans. Consum. Electron.*, vol. 69, no. 3, pp. 640–648, Aug. 2023, doi: 10.1109/TCE.2023.3267836.
[34] D. Pinardi, N. Rocchi, A. Toscani, M. Binelli, G. Chiorboli, A. Farina, and L. Cattani, "An innovative architecture of full-digital microphone arrays over A^2B network for consumer electronics," *IEEE Trans. Consum. Electron.*, vol. 68, no. 3, pp. 200–208, Aug. 2022, doi: 10.1109/TCE.2022.3187453.
[35] N. Rocchi, A. Toscani, D. Pinardi, M. Binelli, L. Chiesi, A. Farina, E. Bonomi, and L. Tronchin, "A modular, low latency, A^2B-based architecture for distributed multichannel full-digital audio systems," in *Proc. Immersive 3D Audio, Archit. Automot. (I3DA)*, Sep. 2021, pp. 1–8, doi: 10.1109/I3DA48870.2021.9610947.
[36] A. Toscani, N. Rocchi, D. Pinardi, M. Binelli, L. Saccenti, A. Farina, S. Pavoni, and M. Vanali, "Low-cost structural health monitoring system for smart buildings," in *Proc. 2nd Int. Conf. Sustain. Mobility Appl., Renewables Technol. (SMART)*, Nov. 2022, pp. 1–7, doi: 10.1109/SMART55236.2022.9990379.
[37] A. Toscani, N. Rocchi, D. Pinardi, M. Binelli, L. Saccenti, A. Farina, S. Pavoni, and M. Vanali, "Low-cost condition monitoring system for smart buildings and industrial applications," *IEEE Trans. Ind. Appl.*, vol. 60, no. 1, pp. 1870–1878, Feb. 2024, doi: 10.1109/TIA.2023.3326784.
[38] A. Toscani et al., Mar. 28, 2024, "Resource data for system validation," IEEE Dataport, doi: 10.21227/rsq0-0840.
[39] A. Toscani et al., Mar. 28, 2024, "Resource data for accelerated bearing test," IEEE Dataport, doi: 10.21227/yqmb-8h89.
[40] M. M. Tahir, A. Q. Khan, N. Iqbal, A. Hussain, and S. Badshah, "Enhancing fault classification accuracy of ball bearing using central tendency based time domain features," *IEEE Access*, vol. 5, pp. 72–83, 2017, doi: 10.1109/ACCESS.2016.2608505.
[41] R. B. Randall, "Noise and vibration data analysis," in *Handbook of Noise and Vibration Control*, M. J. Crocker, Ed., Hoboken, NJ, USA: Wiley, 2007, doi: 10.1002/9780470209707.

DANIEL PINARDI received the M.S. degree (cum laude) in mechanical engineering and the Ph.D. degree (Doctor Europaeus) in industrial engineering from the University of Parma, Italy, in July 2016 and March 2020, respectively. His M.S. thesis on loudspeaker modeling and the Ph.D. thesis on the design of microphone, hydrophone, and camera arrays for spatial audio and video recording. He has been a Research Assistant of Prof. Angelo Farina with the University of Parma, since 2016. His research interests include spatial audio, design of transducer arrays, acoustics simulations and 3D auralization, applied to automotive field, and underwater acoustics.

LUCA ARPA received the M.S. degree in mechanical engineering from the University of Ferrara, Italy, in 2023, with a thesis on rolling element bearing prognostic using machine learning methodologies to predict the remaining useful life. He has been working for one year as a Research Assistant with the Research Group of Applied Mechanics, Department of Engineering, University of Ferrara. His research interests include machine diagnostics, data-driven prognostics, and vibrational characterization of mechanical systems for condition monitoring.

ANDREA TOSCANI received the M.S. degree (cum laude) in electronic engineering and the Ph.D. degree in information technology from the University of Parma, Italy, in 2004 and 2008, respectively.

Since 2004, he has been working with the Department of Information Engineering (now, the Department of Engineering and Architecture), University of Parma, where he is currently a Research Fellow. He is the author of three patents. His research interests include power electronics, high-performance electric drives, diagnostic techniques for industrial electric systems, and power converter for audio application.

ELISABETTA MANCONI received the M.S. degree in mechanical engineering from the University of Parma, in 2002, the European Doctorate degree in sound and vibration from ISVR, Southampton, U.K., in 2007, and the Ph.D. degree in industrial engineering from the University of Parma, in 2008. She has been an Associate Professor with the University of Parma, since 2019. Her research interests include methods for predicting structural vibrations, wave propagation, and band-gap formations in waveguides and periodic structures.

MARCO BINELLI received the B.S. and M.S. degrees in electronic engineering and the Ph.D. degree from the University of Parma, Italy, in 2003, 2006, and 2010, respectively. Since 2010, he has been a Research Fellow with the University of Parma. His research interests include equalization, microphones and loudspeakers arrays, spatial audio psychoacoustics, and active noise control.

EMILIANO MUCCHI received the M.S. degree (cum laude) in mechanical engineering and the Ph.D. degree in mechanics of machines from the University of Ferrara, in 2003 and 2007, respectively.

He was an Assistant Professor at with the University of Ferrara, from 2010 to 2017, where he has been an Associate Professor, since 2018. His scientific activity is centred in the field of noise and vibrations of machines, with reference to elastodynamic models, condition monitoring, diagnostics, and experimental vibration measurements. He has been a Principal Investigator of several national and international peer review projects in the last ten years, author and co-author of more than 130 papers, and an Editor of International Journals: *Mathematical Problems in Engineering*, *Shock and Vibration*, *Vibration and Acoustics Research Journal*.

Open Access funding provided by 'Università degli Studi di Parma' within the CRUI CARE Agreement